Séminaire CosmoObs - LPSC

CHEX-MATE: Unveiling the connection between Cluster Mergers and Diffuse Radio Emission from Weak Lensing

Lorenzo Ingoglia
INAF - IRA, Bologna
June 5, 2026

In collaboration with R. Cassano, C. Giocoli, R. Gavazzi, K. Umetsu, M. Balboni, and others

Galaxy clusters as astrophysical and cosmological probes

- Massive DM halo host **galaxy clusters**
- Measuring their **mass** is crucial for **cosmology** and **astrophysic**
- Their mass is distributed among: **Galaxies** (less than 5-10%), **ICM** (~10-15%), and **DM** (85%)
- Clusters are **dynamic systems** that grow through energic merger events, triggering **diffuse synchrotron radio emission**, observed as radio halos and relics

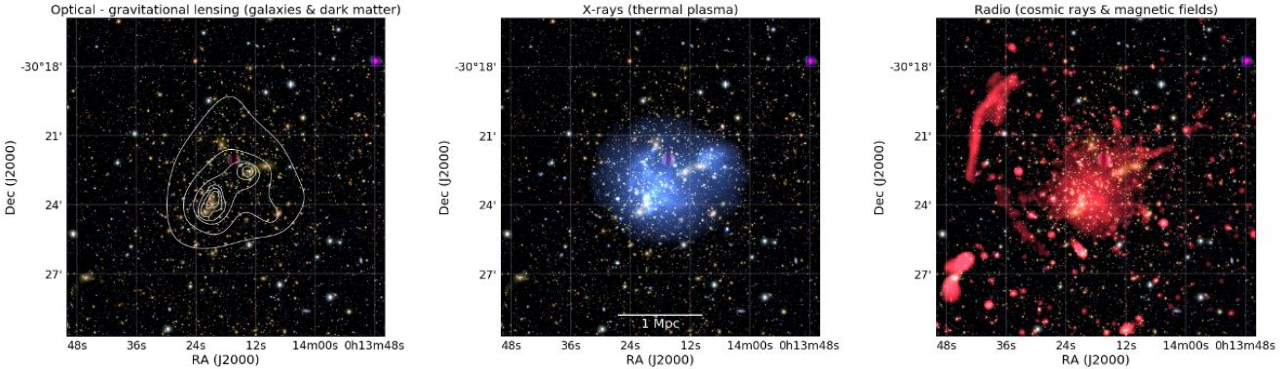

Optical + DM (Subaru) | Optical (Subaru) + X-ray (Chandra) | Optical (Subaru) + Radio (VLA)

Visible, DM, X-ray and Radio components distribution in Abell 2744
Credits: vanWeeren+19

Radio diffuse emissions in clusters

	RH	RR
host state	disturbed	disturbed
location	centre	outskirts
morphology	roundish	elongated
size (Mpc)	∼0.3–2	∼0.3–2
α	∼1–1.5	∼1–1.5
origin	turbulence	shocks

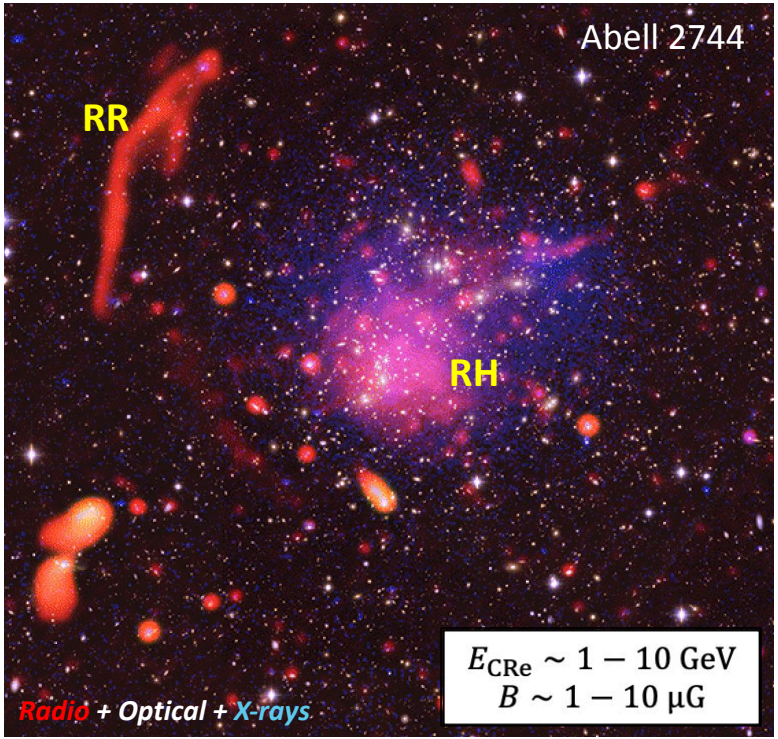

Credits: Pearce et al.; Bill Saxton, NRAO/AUI/NSF; Chandra; Subaru; ESO

Radio halo - merger connection ?

- Diffuse synchrotron **radio emission** in clusters (radio halos and relics) is often linked to **merging events** (X-ray)
- Turbulence from cluster mergers re-accelerates relativistic electrons in the ICM to produce the observed radio emission (e.g. Brunetti&Jones+14)
- LOFAR has detected radio halos in **less** dynamically disturbed systems, while also revealing several merging clusters **without** diffuse emission.

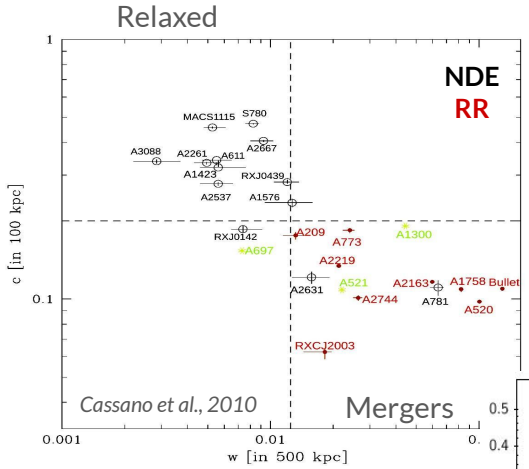

Then GMRT 600 MHz

Now, LOFAR, 150 MHz

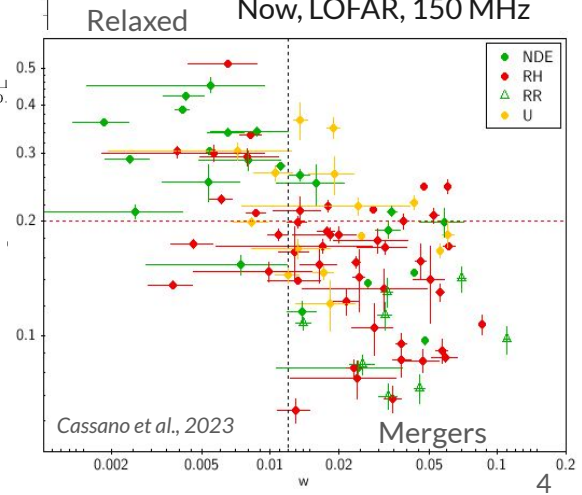

Light concentration vs centroid shift
Credits: Cassano+10 (Top)
Cassano+23 (Right)

Weak Lensing to observe cluster's total mass

- **Gravitational lensing** is the most unbiased method to measure the **total mass** of galaxy clusters
- The **lens** (cluster) deflects the light of background **sources** (galaxies)
- The **projected mass distribution** can be recovered by measuring the **lensing signal**
- Lensing projects the mass of all structures along the line of sight (2D measurements)

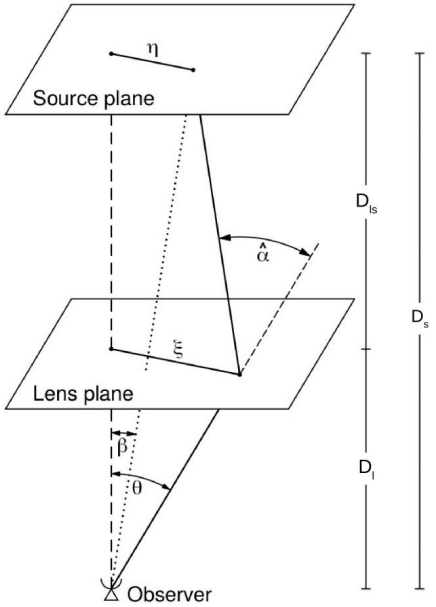

Diagram of a typical lens system
Credits: Bartelmann&Schneider01

Weak Lensing to observe cluster's total mass

- Source shape is deformed by **convergence** (isotropic) and **shear** (anisotropic)
- Cluster mass distribution is encoded in the **convergence** (surface density) and the **tangential shear** (excess surface density)
- **Strong lensing**: effect strong enough to produce arcs or multiple images, closed to the center
- **Weak lensing**: weak source deformations but numerous objects, the signal can be computed up to large scales (~ 10 Mpc)
- In WL, ellipticity and (reduced) shear are equivalent

Illustration of the effects of the convergence and the shear
(*Credits: Bartelmann&Schneider01*)

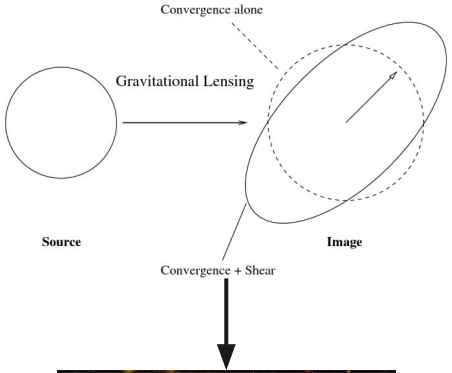

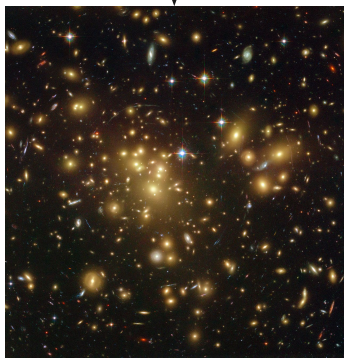

Galaxy cluster Abell 1689 from HST
Credits: NASA/ESA

Weak Lensing to observe cluster's total mass

- In WL, intrinsic shape has to be filtered out
- To correct for statistical fluctuations, source ellipticities are **stacked in radial bins**
- Shear is stacked over cluster bins assuming a **weighting average** $\gamma_j \simeq \frac{\sum_{i\in j} w_i \epsilon_i}{\sum_{i\in j} w_i}$
- Shear is measured in radial bin for **higher SNR** profiles

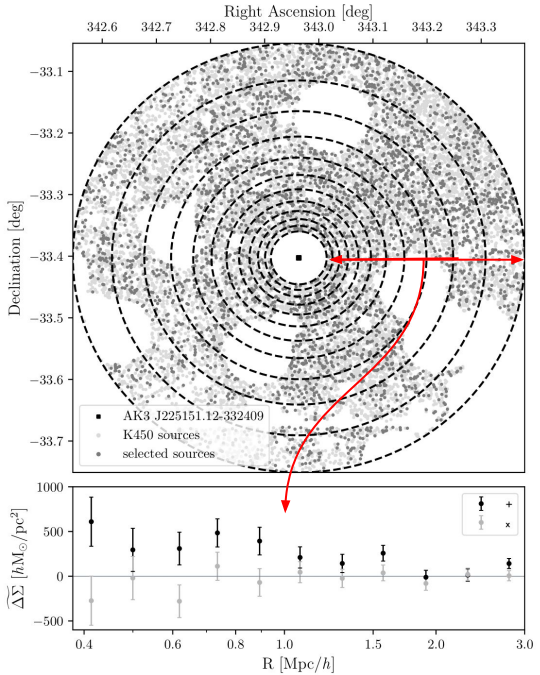

Lensing signal stacked over annuli (AMICO + KiDS-DR3)
Credits: Ingoglia+22

Unveiling cluster mergers with WL

- WL on clusters measures the total mass distribution **regardless its dynamical state**
- WL shows cluster's mass on large scales where **non-thermal** components have an important role
- **2D reconstructed mass maps** show the **anisotropy** of the matter distribution in mergers
- **1D surface density profiles** show the **isotropic** distribution in radial apertures and serve to constrain **cluster properties** by model fitting
- Comparing the **maps and profiles** of clusters with and without diffuse radio emissions could **unveil** how the overall matter distribution influence the formation of **thermal and non-thermal emissions** in clusters

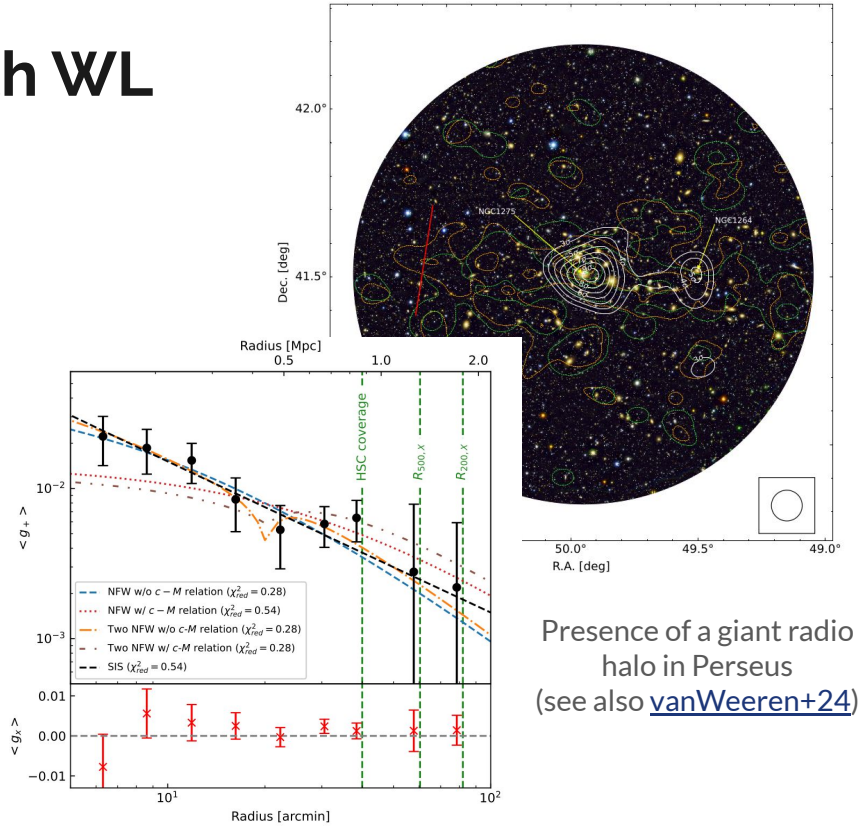

Presence of a giant radio halo in Perseus (see also vanWeeren+24)

Dark matter and galaxy distribution of the Perseus cluster (Top)
Reduced shear profile of the Perseus cluster (Bottom)
Credits: HyeongHan+24

CHEX-MATE / LOFAR / MeerKAT / Euclid coverages

- **Sample selection**
  - 33 CHEX-MATE clusters
  - covered in radio + weak lensing data
- **Radio observations**
  - LOFAR (LoTSS-DR3, low frequency)
  - MeerKAT (high frequency)
- **Weak lensing data**
  - SuprimeCam (Subaru), HSC, Megacam (CFHT) and Omegacam (VST) images and compiled in the **AMALGAM2** database
  - Shape catalogues produced with **SourceXtractor++**
  - Gavazzi et al., in prep. Umetsu et al., in prep.

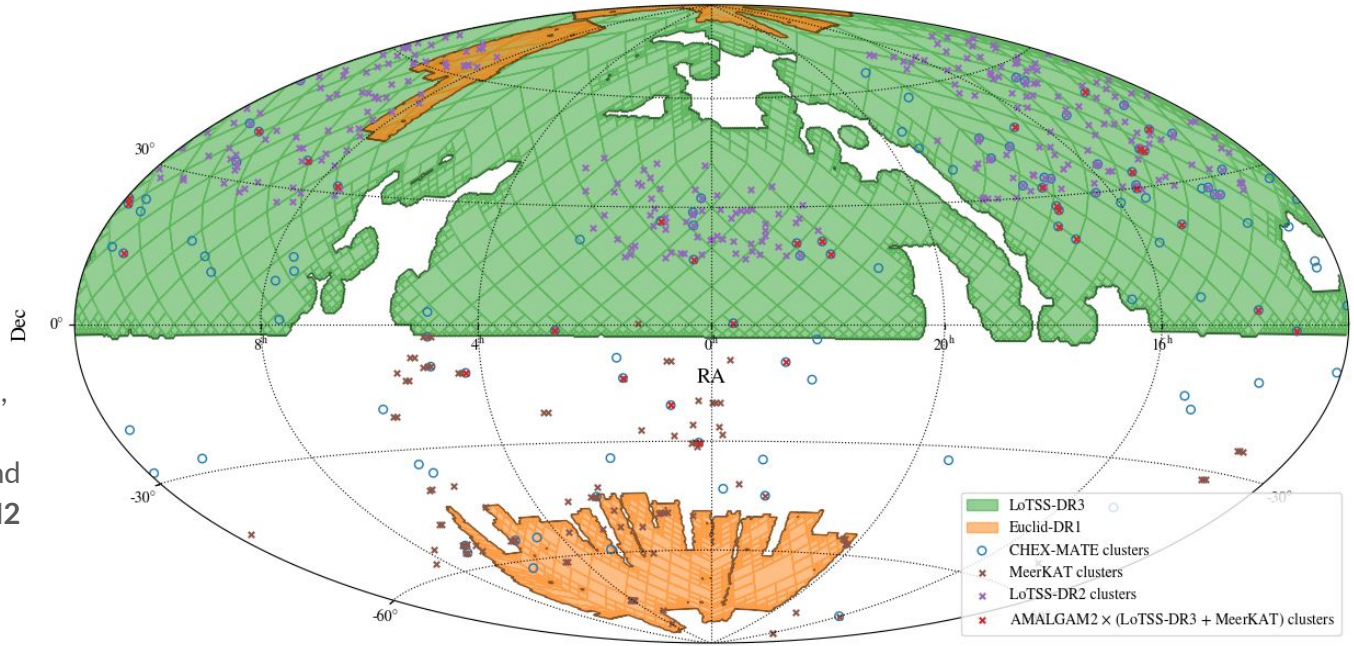

Note: LoTSS covers Euclid-DR1 in the north, some MeerKAT observations in the south. No coverage with CHEX-MATE, but X-ray/SZ observations to be complete with eRASS and SPT

Selection of CHEX-MATE clusters

- **Total sample**: 118 clusters
- **Radio coverage**: 95 clusters (80%)
- **WL coverage**: 41 clusters (35%)
- Joint sample (Radio + WL): 33 clusters (28%)
  - LoTSS: 26
  - MeerKAAT: 7
- Clusters with WL evenly distributed across Tiers 1/2 (low / high mass-redshift bins)
- Large majority (31 / 33) of clusters are measured with $SNR_{WL} > 3$

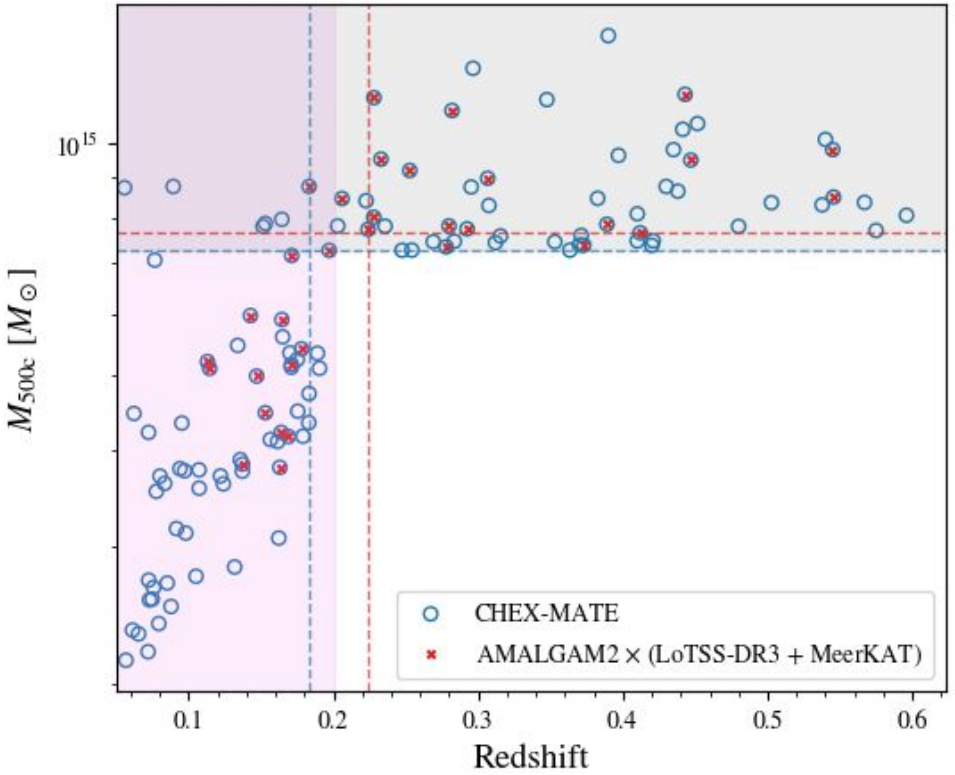

X-ray morphological disturbance

- Cluster morphology quantified using two X-ray indicators:
  - **Centroid shift (w):** X-ray peak–centroid scatter in multiple apertures
  - **Concentration (c):** surface brightness ratio within 0.15–R_{500}
- Morphological parameter **M** combines 4 morphological parameters (see Campitiello+22)
- Disturbance parameter **D** better rely on the (c, w) space (see Cuciti+23)
  - defined from projection in the (c, w) space
  - provides a continuous measure of the dynamical state
- We categorize our sample into relaxed and disturbed samples from the **median** of the disturbance on the AMALGAM2

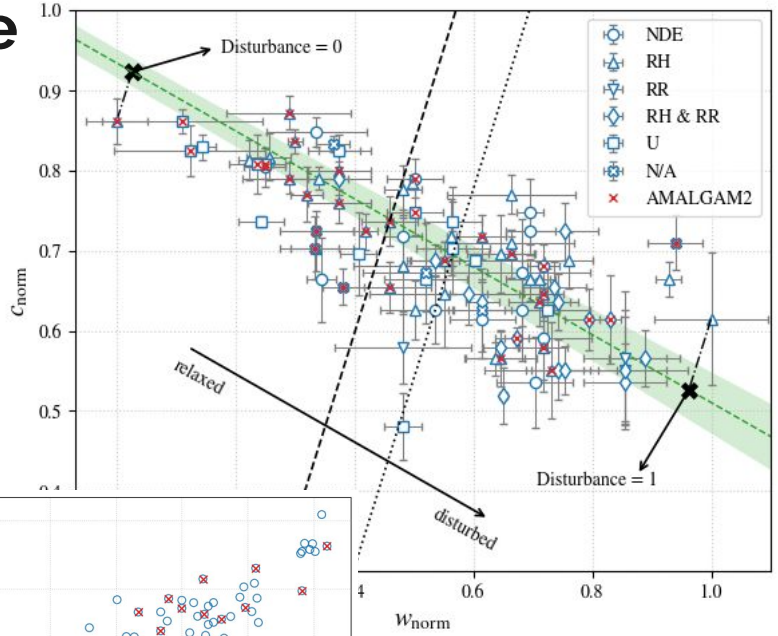

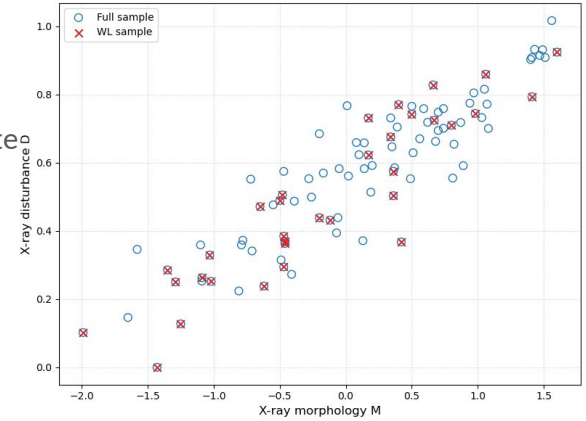

Radio classification in the CHEX-MATE samples

- Cluster grouped by radio classification
  - **RH**: Radio Halo
  - **RR**: Radio Relic
  - **NDE**: No Diffuse Emission
  - **U**: Uncertain
  - **N/A**: Not Avalaible data
- In the AMALGAM2:
  - low number of NDE
  - high fraction of RH
- RH size based on:
  - measured effective radius (R_e)
  - visual inspection
- RH classified into:
  - **Mini** (core concentrated)
  - **Giant** (Mpc scale)

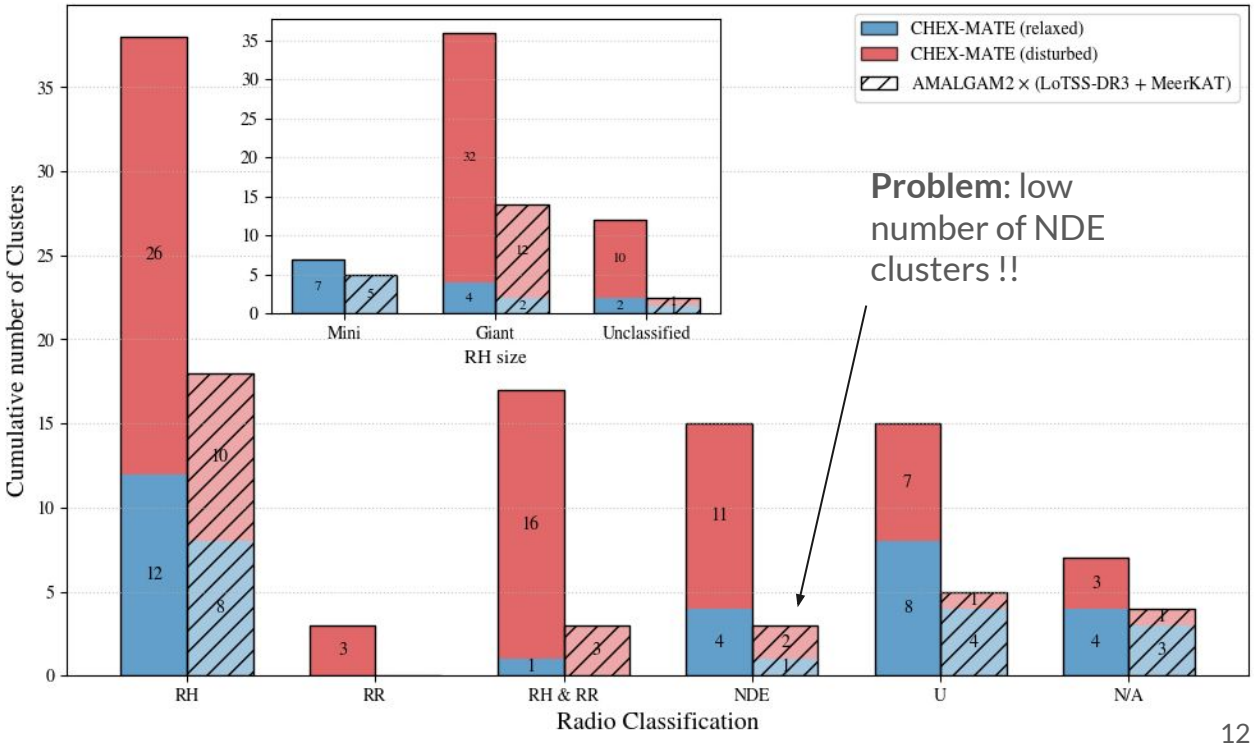

Single 1D + 2D WL

- Selection of sources based in colour and cluster membership score S_{mem}
- Resolution of the smoothing scale set with a fixed galaxy density $\mathbf{n_{gal} = 15\,\sigma_G^{-1}}$
- Convergence reconstructed from shears with a Kaiser&Squire+93 inversion method in Fourier space
- Shear profile measured with **BMO+2h** term (Tinker+10), with LSS covariance
- Qualitative checks with AMALGAM2 and *Umetsu et al, in prep.* mass maps
- Measurement of DM peaks
  - SNR_{KE} peak regions are detected for SNR > 3 (fixed noise from the std of the B-mode), within R_{500}
  - WL centers are measured with centroid SNR_{KE} within the detected region

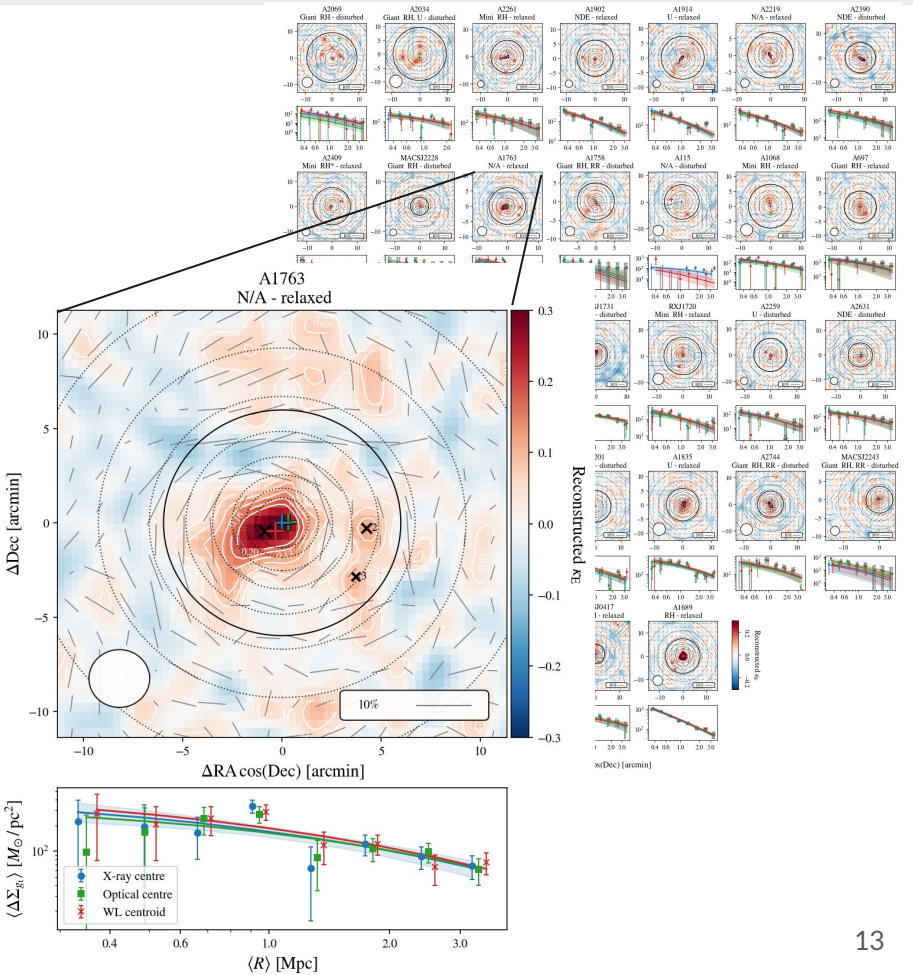

Maps for high SNR_{KE} < R_{500} clusters

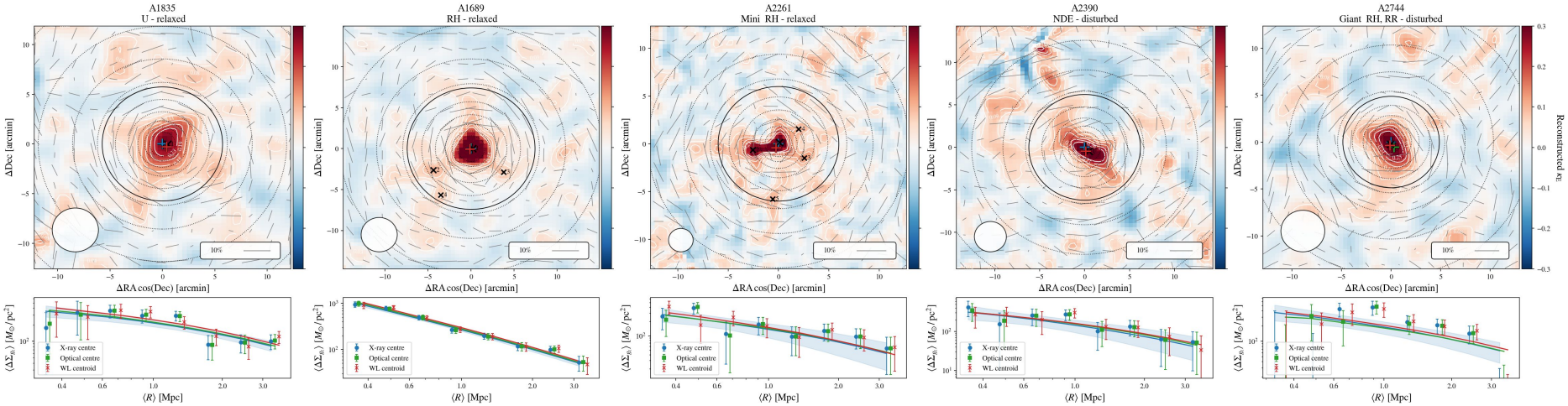

Relaxed → Disturbed

Some examples: RXJ1720

- Redshift: 0.1644
- Tier: 1
- Disturbance: 0.000
- Map resolution: 76.72 kpc
- Galaxy number density (<R_{500}): 5.298 arcmin
- SNR_{KE} (<R_{500}): 3.10
- Number of detection (<R_{500}): 2
- log M_{200c} / 1e14 M_{sun}: 0.755±0.223
- log c_{200c}: 0.723±0.459

- Biava+21:
  - Hosts both a central mini halo and a giant halo
  - Ultra-steep spectrum with $\alpha_{54}^{144} \sim 3.2$,

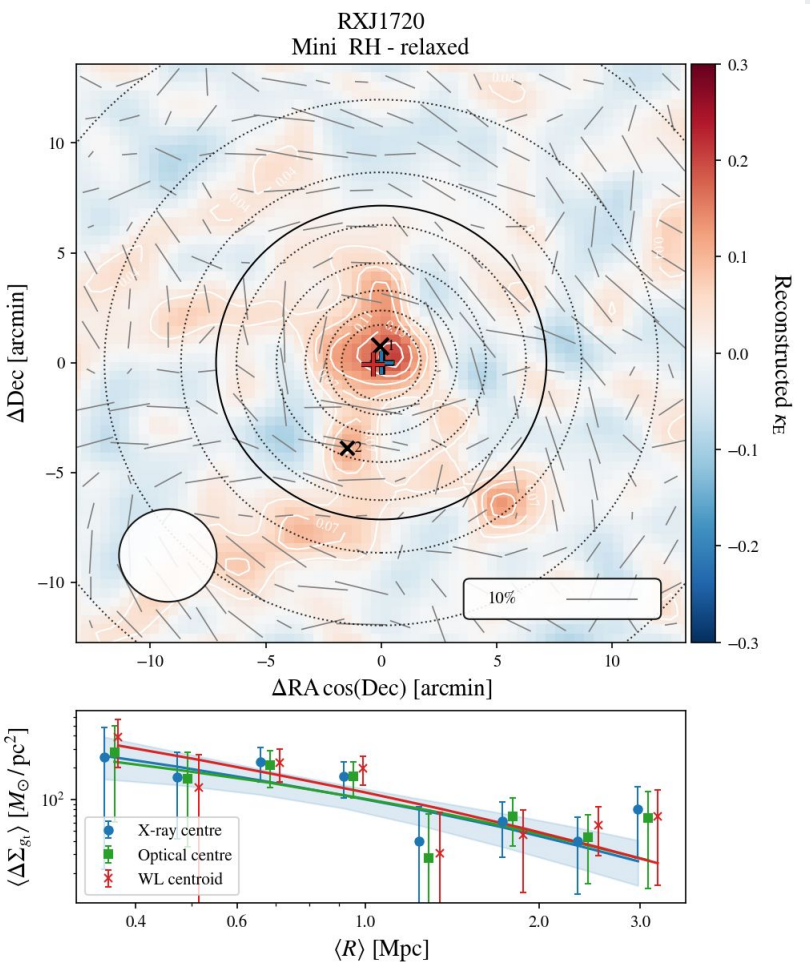

Some examples: A1835

- Redshift: 0.2528
- Tier: 2
- Disturbance: 0.102
- Map resolution: 103.32 kpc
- Galaxy number density (<R_{500}): 5.907 arcmin
- SNR_{KE} (<R_{500}): 7.99
- Number of detection (<R_{500}): 1
- log M_{200c} / 1e14 M_{sun}: 1.420±0.127
- log c_{200c}: 0.337±0.154

- Murgia+09:
  - Presence of a mini-halo, classified as a relaxed, cooling core galaxy cluster

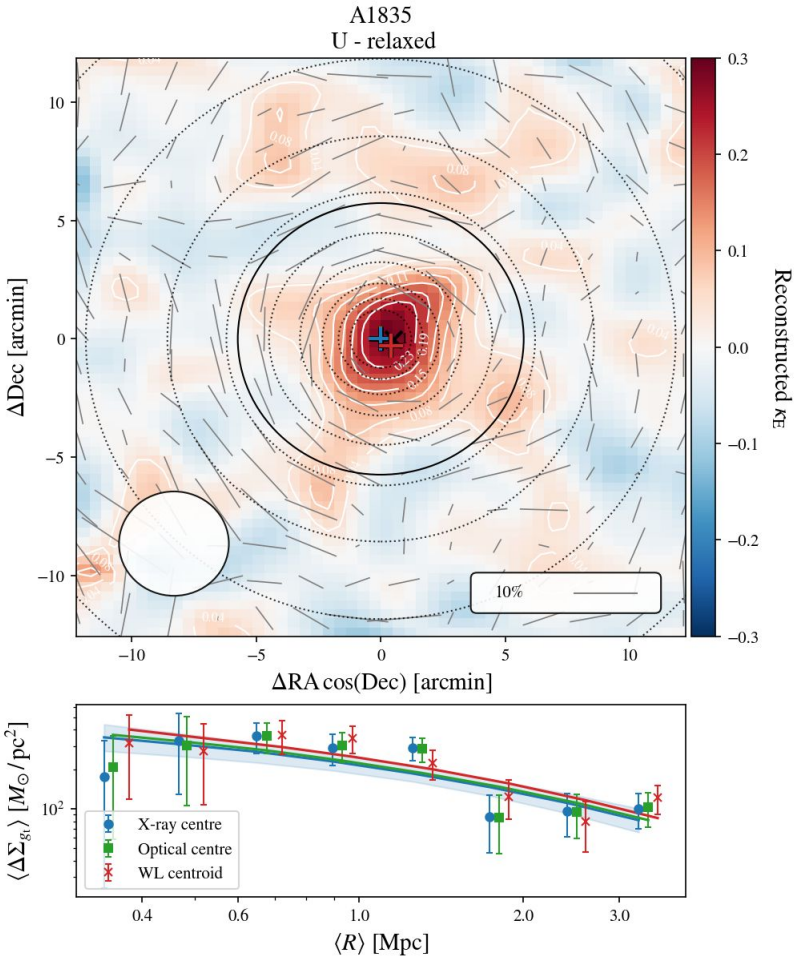

Some examples: A1689

- Redshift: 0.1832
- Tier: 2
- Disturbance: 0.286
- Map resolution: 88.97 kpc
- Galaxy number density ($<R_{500}$): 15.28 arcmin
- SNR_{KE} ($<R_{500}$): 6.99
- Number of detection ($<R_{500}$): 3
- log M_{200c} / 1e14 M_{sun}: 1.170±0.069
- log c_{200c}: 1.168±0.152

- Vacca+11:
  - Extended, diffuse, low-surface brightness radio emission located in the central region
- Chappuis+25:
  - Large WL / X-ray mass discrepancy
  - Strongly elongated along the line of sight

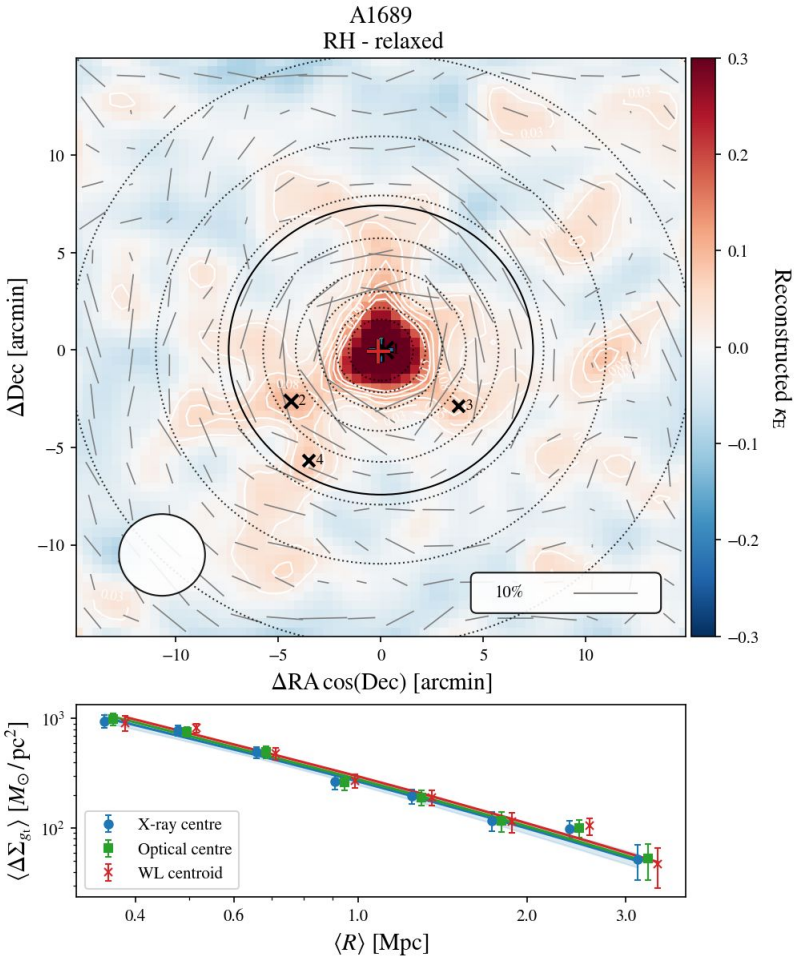

Some examples: A1413

- Redshift: 0.1427
- Tier: 1
- Disturbance: 0.295
- Map resolution: 65.95 kpc
- Galaxy number density (<R_{500}): 17.843 arcmin
- SNR_{KE} (<R_{500}): 4.99
- Number of detection (<R_{500}): 2
- log M_{200c} / 1e14 M_{sun}: 0.949±0.154
- log c_{200c}: 0.644±0.234

- Savini+19, Riseley+2023, and Luseti+24:
  - Mini-halo extending up to 584 kpc and spectral index −1.01 ± 0.06 (MeerKAT L-band 872–1712 MHz)
  - Moderately-disturbed non-cool-core cluster

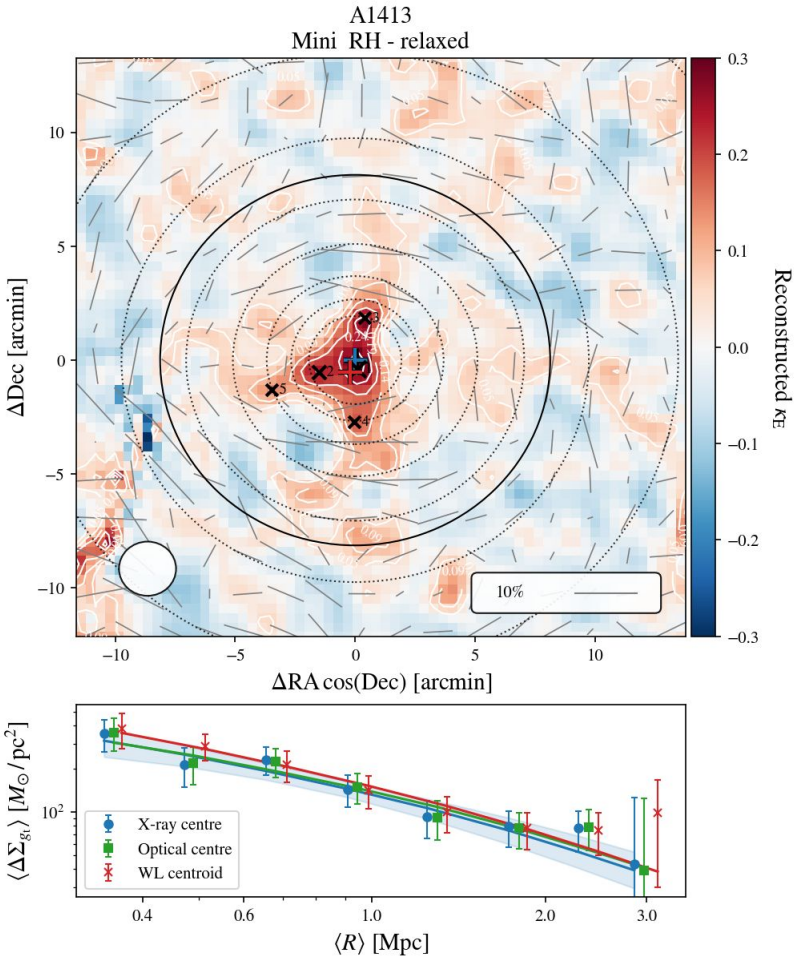

Some examples: A2261

- Redshift: 0.224
- Tier: 2
- Disturbance: 0.369
- Map resolution: 100.21 kpc
- Galaxy number density ($<R_{500}$): 13.784 arcmin
- SNR_{KE} ($<R_{500}$): 7.32
- Number of detection ($<R_{500}$): 3
- log M_{200c} / 1e14 M_{sun}: 1.027±0.334
- log c_{200c}: 0.470±0.379

- Sommer+17 and Botteon+22:
  - Detection of the presence of megaparsec-scale radio emission identified as a mini radio halo

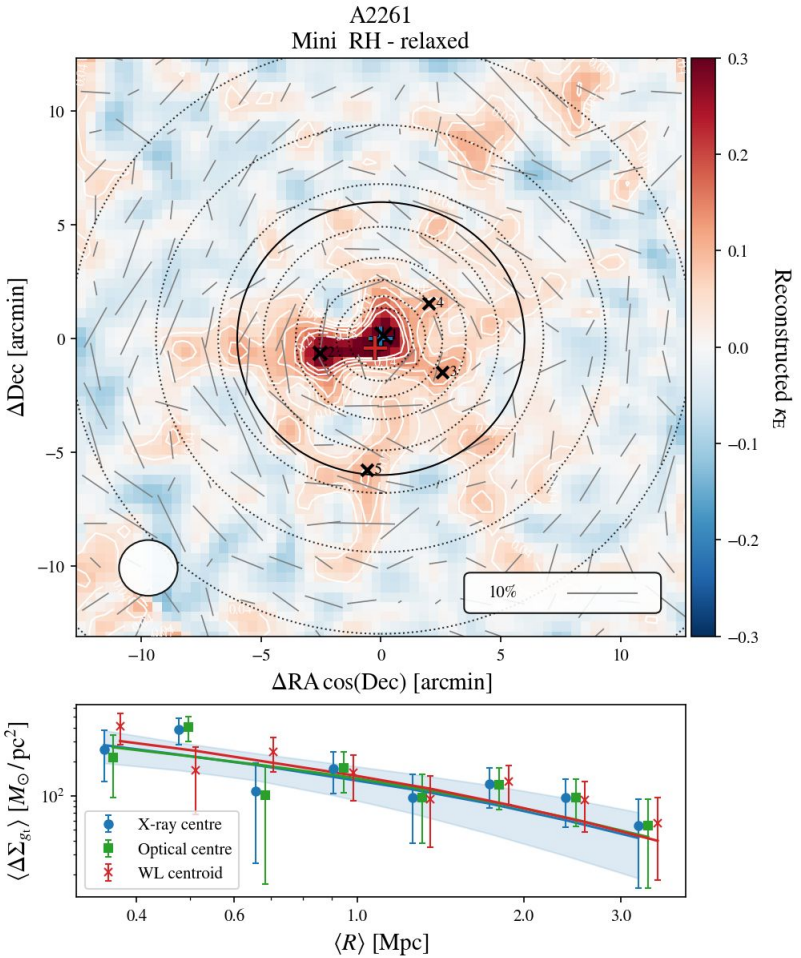

Some examples: A697

- Redshift: 0.282
- Tier: 2
- Disturbance: 0.439
- Map resolution: 120.44 kpc
- Galaxy number density (<R_{500}): 11.614 arcmin
- SNR_{KE} (<R_{500}): 6.06
- Number of detection (<R_{500}): 2
- log M_{200c} / 1e14 M_{sun}: 0.835±0.397
- log c_{200c}: 0.259±0.260

- Macario+10:
  - Radio halo with a very steep spectrum: 1.7-1.8 between 325 MHz and 1.4 GHz

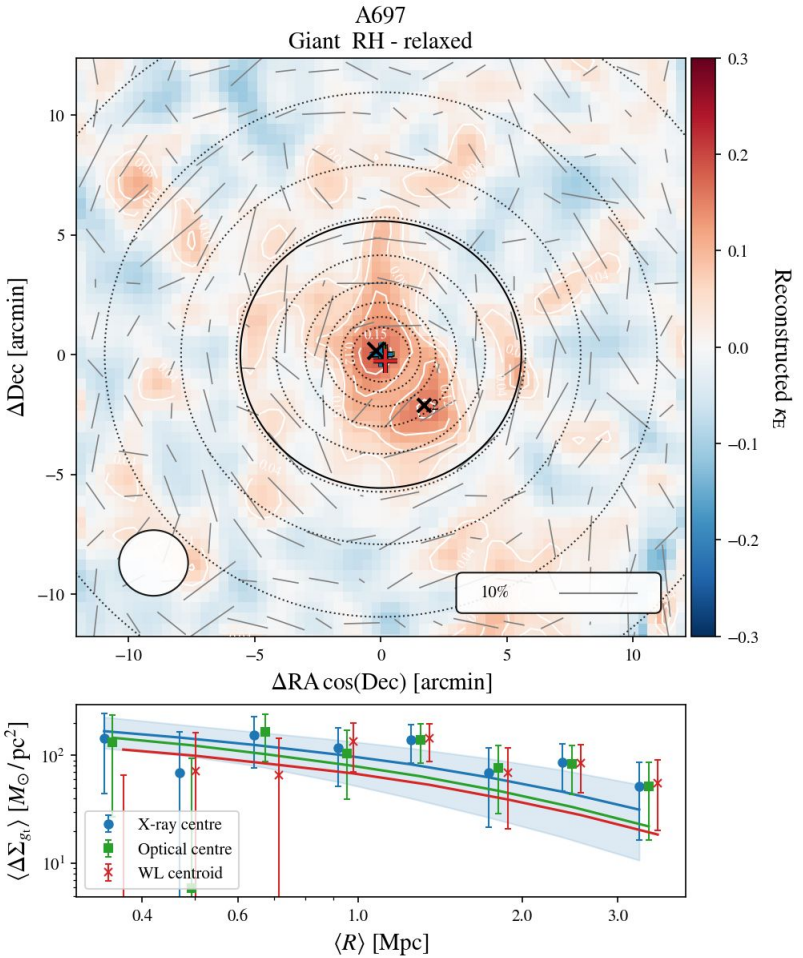

Some examples: A2390

- Redshift: 0.2329
- Tier: 2
- Disturbance: 0.489
- Map resolution: 107.66 kpc
- Galaxy number density (<R_{500}): 8.152 arcmin
- SNR_{KE} (<R_{500}): 6.74
- Number of detection (<R_{500}): 1
- log M_{200c} / 1e14 M_{sun}: 1.034±0.345
- log c_{200c}: 0.517±0.385

- Botteon+22:
  - Radio halo reinterpreted as lobes of the central AGN

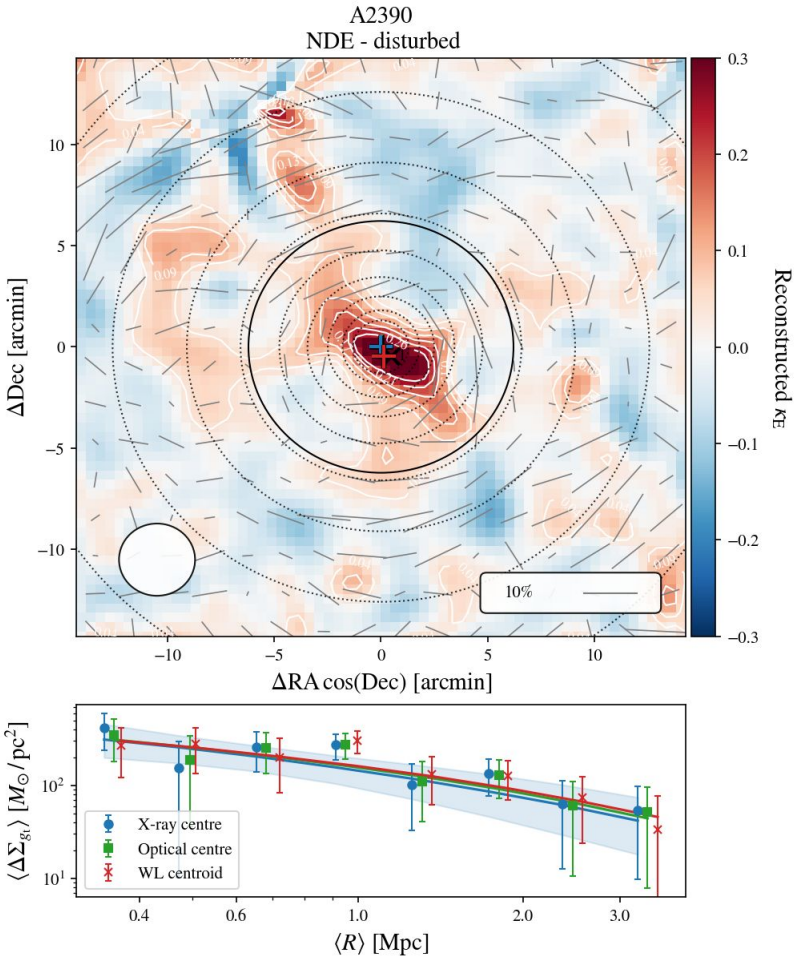

Some examples: A370

- Redshift: 0.373
- Tier: 2
- Disturbance: 0.503
- Map resolution: 149.21 kpc
- Galaxy number density ($<R_{500}$): 6.489 arcmin
- SNR_{KE} ($<R_{500}$): 10.53
- Number of detection ($<R_{500}$): 1
- log M_{200c} / 1e14 M_{sun}: 1.499±0.103
- log c_{200c}: 0.787±0.146

- Xie+20:
  - Faint radio halo (~500–700 kpc) located mostly in the southern part
  - Spectral index of −0.94 ± 0.08 between 325 MHz and 1.5 GHz and −1.77 ± 0.20 between. 1.5 and 3.0 GHz
  - Bimodal mass distribution + X-ray shock/cold-front features indicate an ongoing major merger

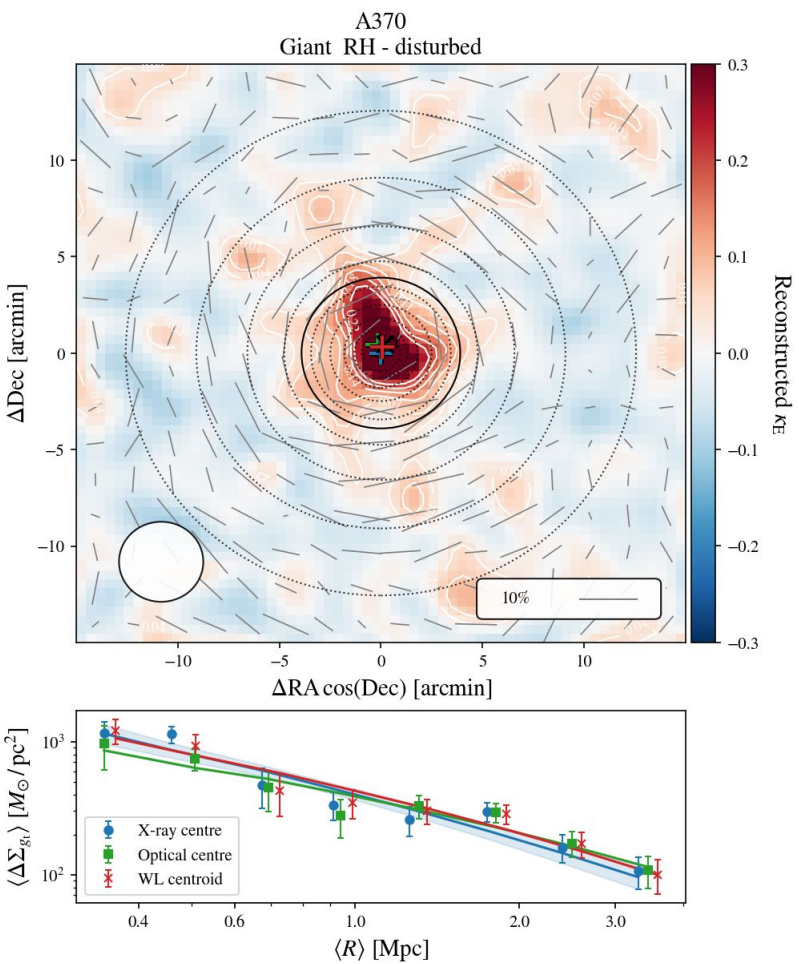

Some examples: A209

- Redshift: 0.206
- Tier: 2
- Disturbance: 0.623
- Map resolution: 96.09 kpc
- Galaxy number density (<R_{500}): 18.527 arcmin
- SNR_{KE} (<R_{500}): 7.56
- Number of detection (<R_{500}): 6
- log M_{200c} / 1e14 M_{sun}: 1.145±0.153
- log c_{200c}: 0.173±0.139

- Feng+24:
  - Possible shock front in the northwest direction and a cold front feature in the southeast direction

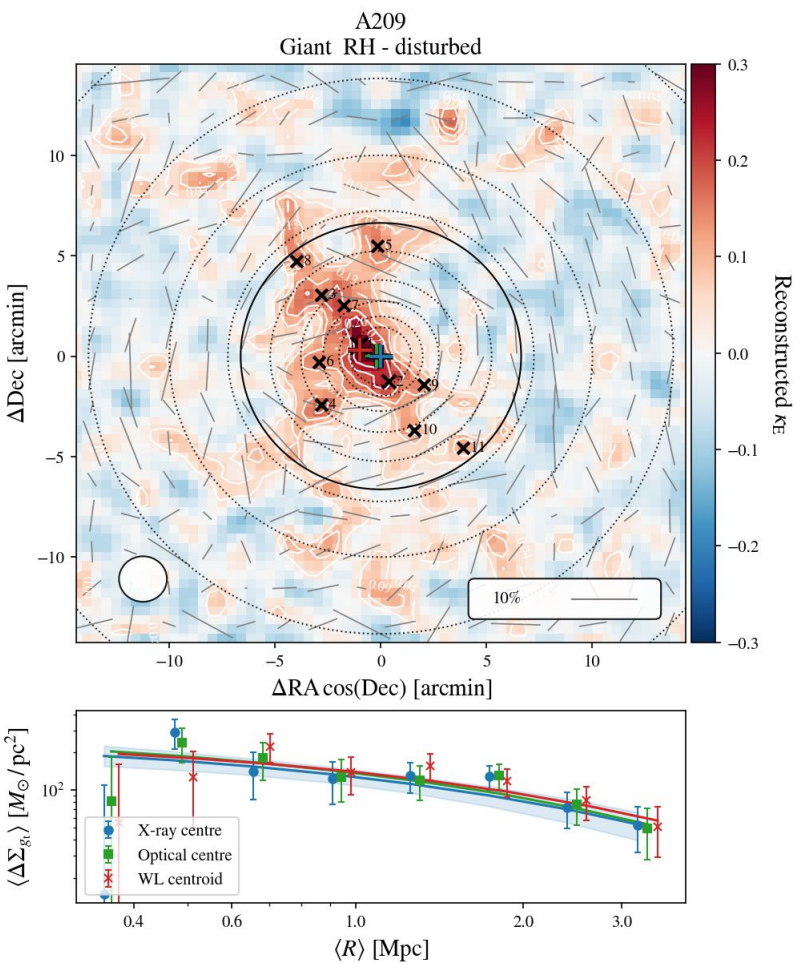

Some examples: A2069

- Redshift: 0.1145
- Tier: 1
- Disturbance: 0.794
- Map resolution: 60.34 kpc
- Galaxy number density (<R_{500}): 4.710 arcmin
- SNR_{KE} (<R_{500}): 2.53
- Number of detection(<R_{500}): 1
- log M_{200c} / 1e14 M_{sun}: 0.157±0.436
- log c_{200c}: 0.735±0.559

- Drabent+15 and Botteon+22:
  - Bimodal cluster with extended emission in both components

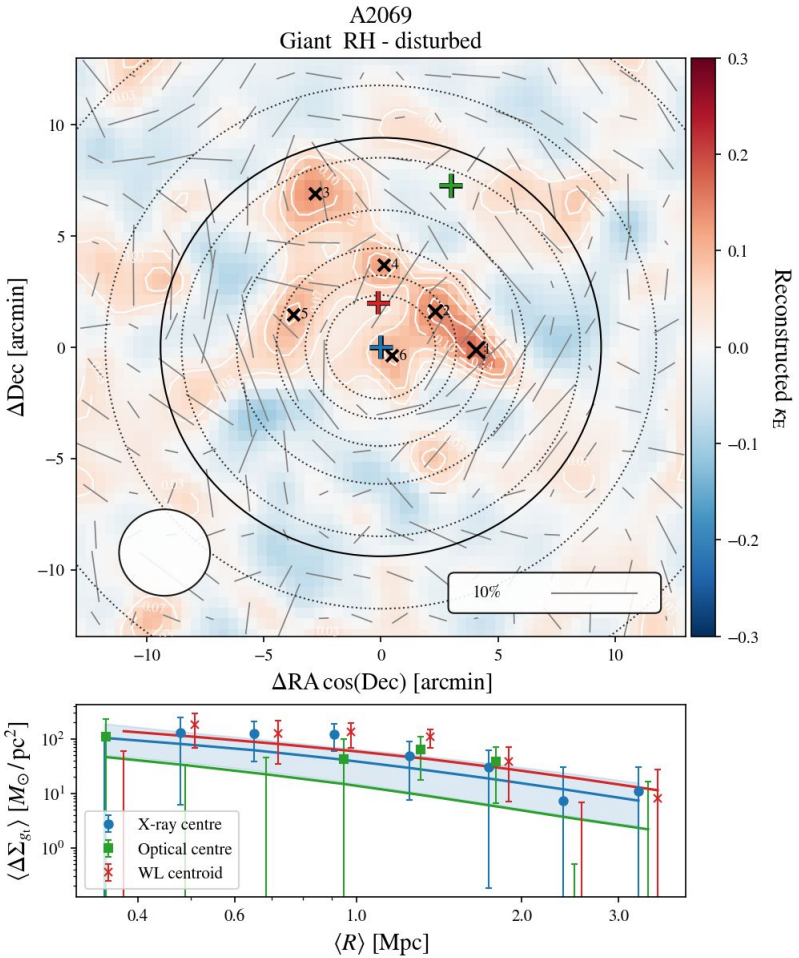

Some examples: A2744

- Redshift: 0.3066
- Tier: 2
- Disturbance: 0.860
- Map resolution: 123.71 kpc
- Galaxy number density (<R_{500}): 4.267 arcmin
- SNR_{KE} (<R_{500}): 8.85
- Number of detection (<R_{500}): 1
- log M_{200c} / 1e14 M_{sun}: 1.267±0.259
- log c_{200c}: 0.387±0.246

- Eckert+16 and Pearce+17:
  - Shock front 1.5 Mpc east of the cluster core
  - Multiple radio relics detections (including the known 1.5 Mpc)

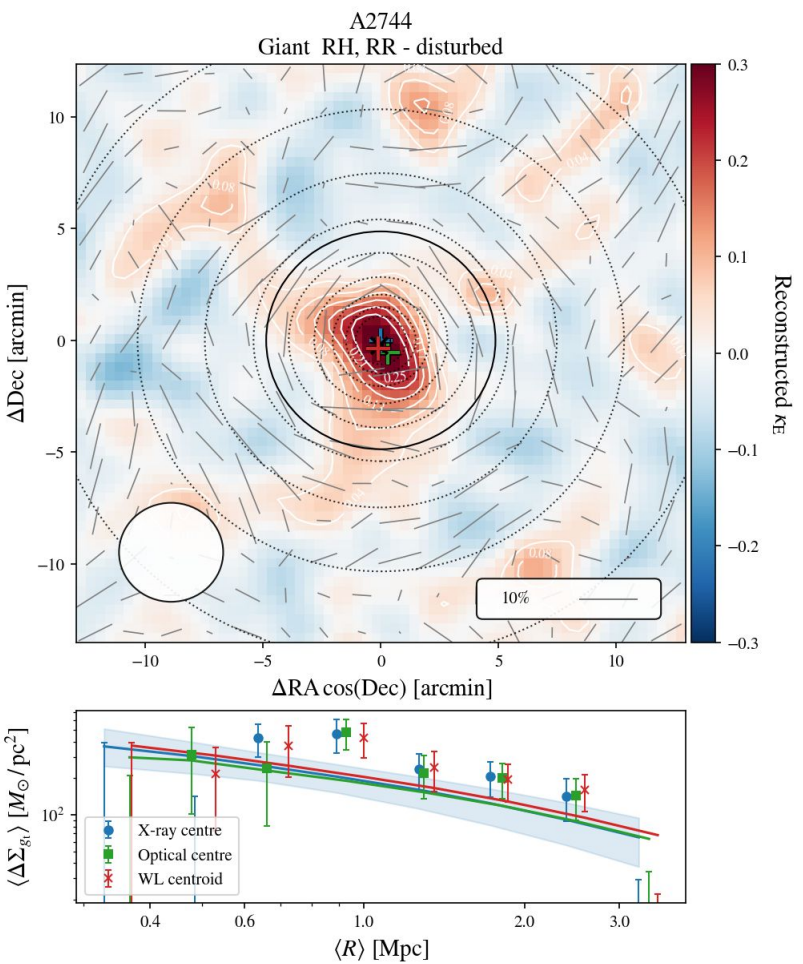

Some examples: A115

- Redshift: 0.1971
- Tier: 1+2
- Disturbance: 0.925
- Map resolution: 88.35 kpc
- Galaxy number density ($<R_{500}$): 6.748 arcmin
- SNR_{KE} ($<R_{500}$): 5.91
- Number of detection ($<R_{500}$): 2
- log M_{200c} / 1e14 M_{sun}: 0.727±0.432
- log c_{200c}: 0.164±0.179

- Beers+1983, Feretti+1984, Barrena+07, and Hallman+18:
  - Single radio relic cluster with double X-ray peaks
  - Two structures identified in the galaxy distribution
  - A hot region was found between the subclusters
- Botteon+16:
  - Co-spatial shock with the radio relic

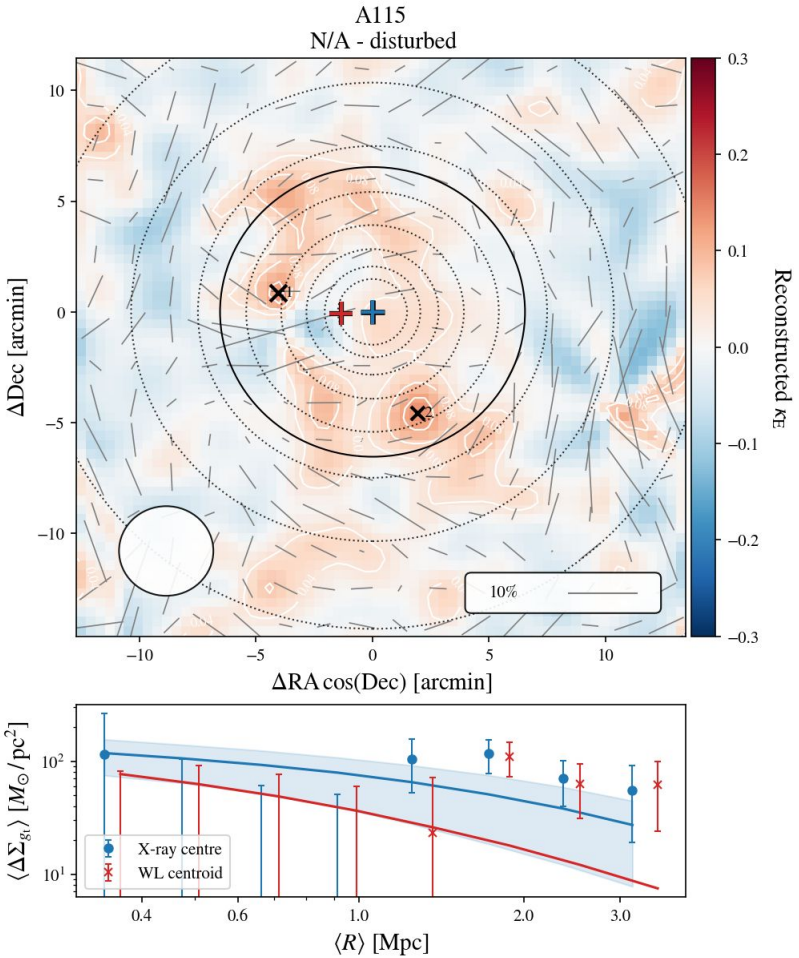

Simulated 3:1 merger

- Cluster mass distribution:
  - 2 eNFW with different 3:1 masses, ellipticity fixed, random orientations
  - Concentration from Diemer&Joyce19
  - Separation from X-ray - BCG
  - K_B from std(K_E)
  - Reduced shear estimate
- AMALGAM2 source mock:
  - Number density
  - Shape noise
  - Source redshift distribution
- Mass reconstruction
  - Mass bias on WL centre (%): -1,8 / -3,0 / 4,8
  - Centre offset to the barycentre vs to the main halo (arcmin): 3,4 vs 1.9 / 1.3 vs 1.5 / 0.1, vs 0.7

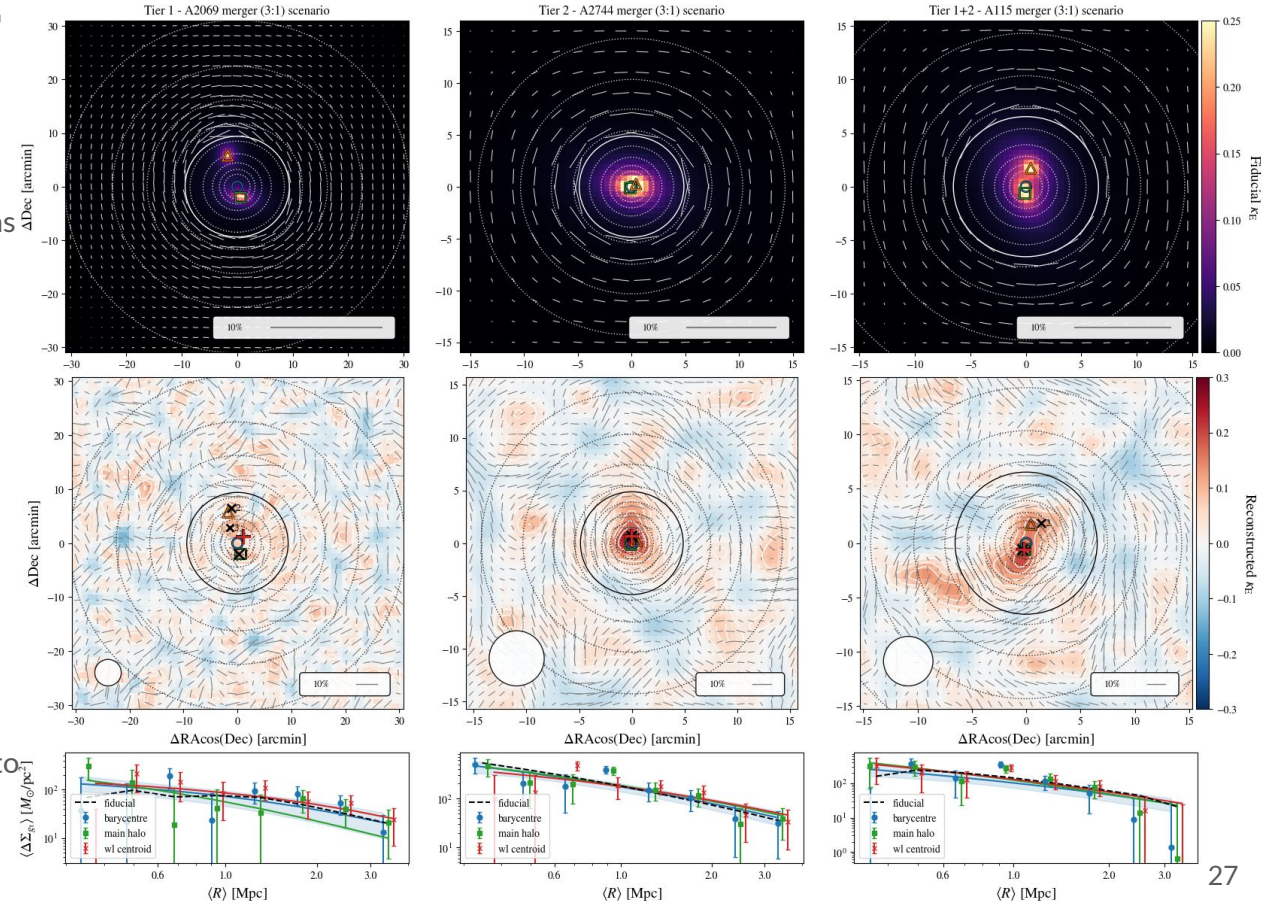

Mass validation with *Umetsu et al.*

Beside the difference in Radial binning, agreement is find with *Umetsu et al., in prep.*:

- Slope: 0.995 ± 0.064
- Intercept: -0.007 ± 0.077
- SNR on the full radial profile agree
- n_{gal} slightly different (+ photo-z cut)

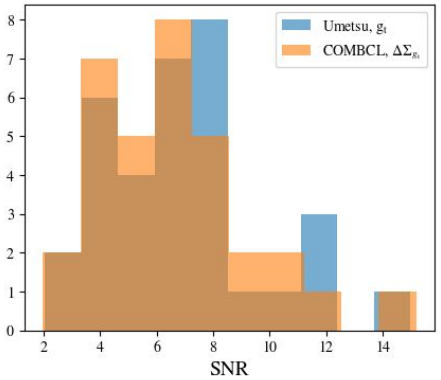

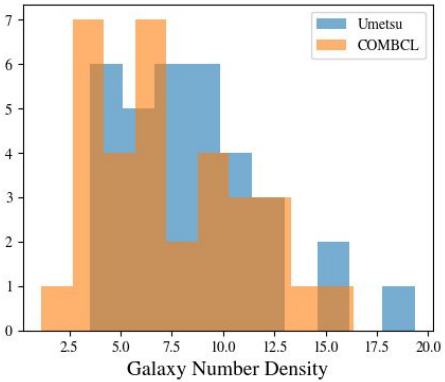

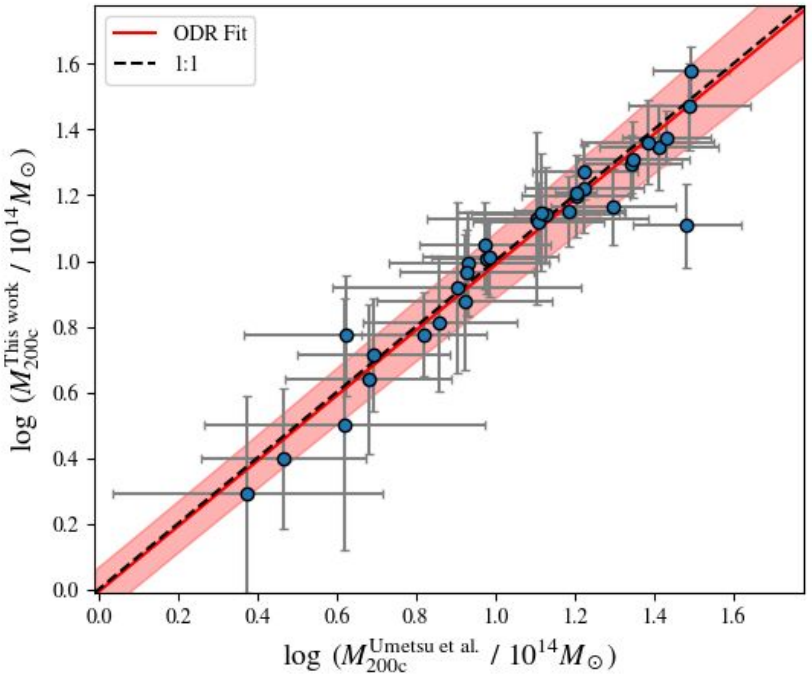

Center offsets from single WL maps

- Angular separation between **X-ray, optical, and WL SNR centres**, in unit of $\mathbf{R_{500,SZ}}$
- Error bars estimated from the SNR centroid std (single detections)
- Center definitions:
  - Optical centre: BCG
  - Xray centre: X-ray peak
  - WL centre: Centroid SNR_{KE} first peak
- Results:
  - Smaller offset found on the Optical vs X-ray centres, **evident median separation for each population**
  - Larger offsets when involving the WL centre due to smoothing effects, but trend repeated
  - **Spearman correlation coefficient and p-value**:
    - WL to Optical: ρ=0.29 / p=0.12
    - WL to X-ray: ρ=0.39 / p=0.02
    - X-ray to Optical: ρ=0.52 / p=0.00

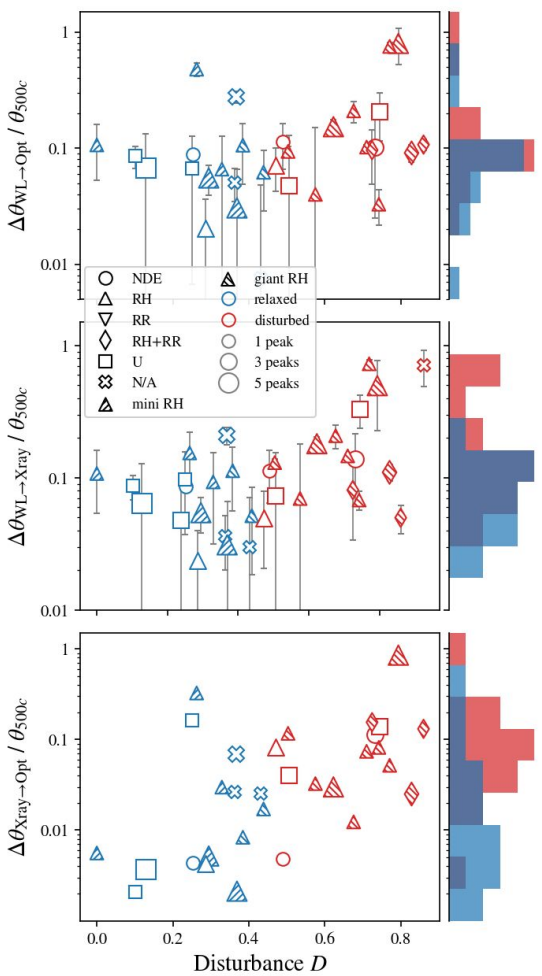

Mass vs concentration from single profiles

- Mass and concentration are **correlated** according to N-body simulations
- **Disturbed** clusters tend to be **less concentrated**
- **Relaxed** clusters in hydrodynamical equilibrium should present **higher concentrations**
- Results:
  - Mass-concentration relation in agreement with simulations
  - ODR fit:
    - Slope: 0.13± 0.17
    - Intercept: 0.36± 0.19
  - Clusters with low disturbance are more massive
  - Clusters with high disturbance covers all the mass range
  - **No correlations observed on concentrations**:
    - Concentration hardly constraint on single profiles (low number of R-bin, low SNR)
  - Need to derive concentrations on stack profiles!!

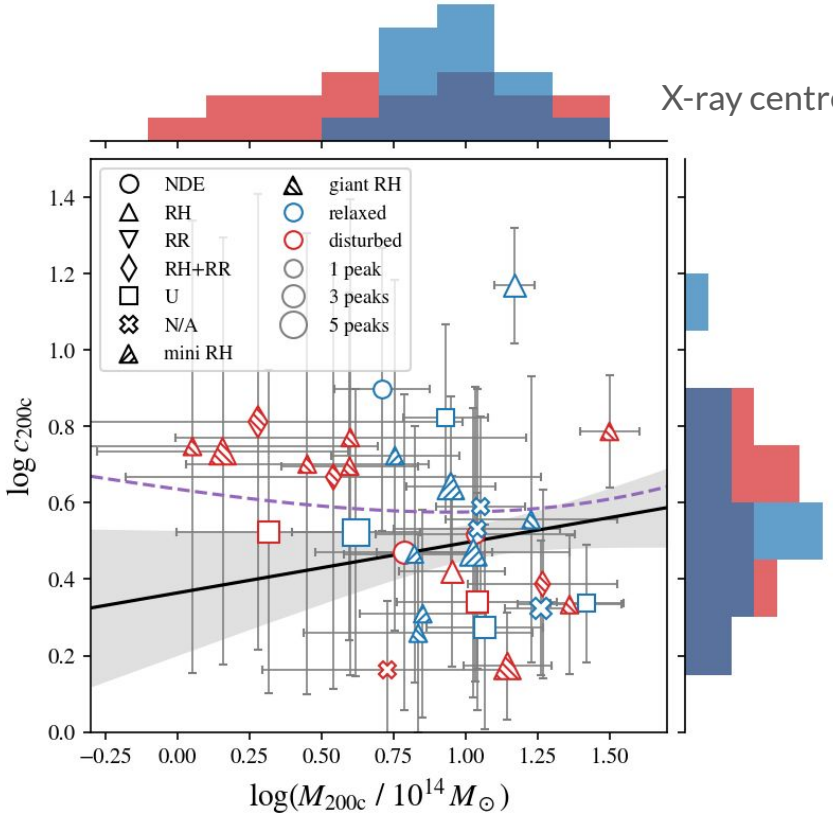

Stacked 1D + 2D WL

- Maps and profiles rescaled to $R_{500,SZ}$ and comoving units, respectively
- Stacked profile account for bootstrap covariance on single profiles
- **BMO + 2h** centred and miscentred models assumed to **break the concentration - σ_{off}- f_{off} degeneracy**, three models were fitted to the measurements:
  - BMO + 2h centred model mass - concentration free
  - BMO + 2h miscentred mass - σ_{off} free + model concentration and f_{off}=1
  - BMO + 2h miscentred mass - f_{off} free + model concentration and σ_{off} fixed to the full sample estimate

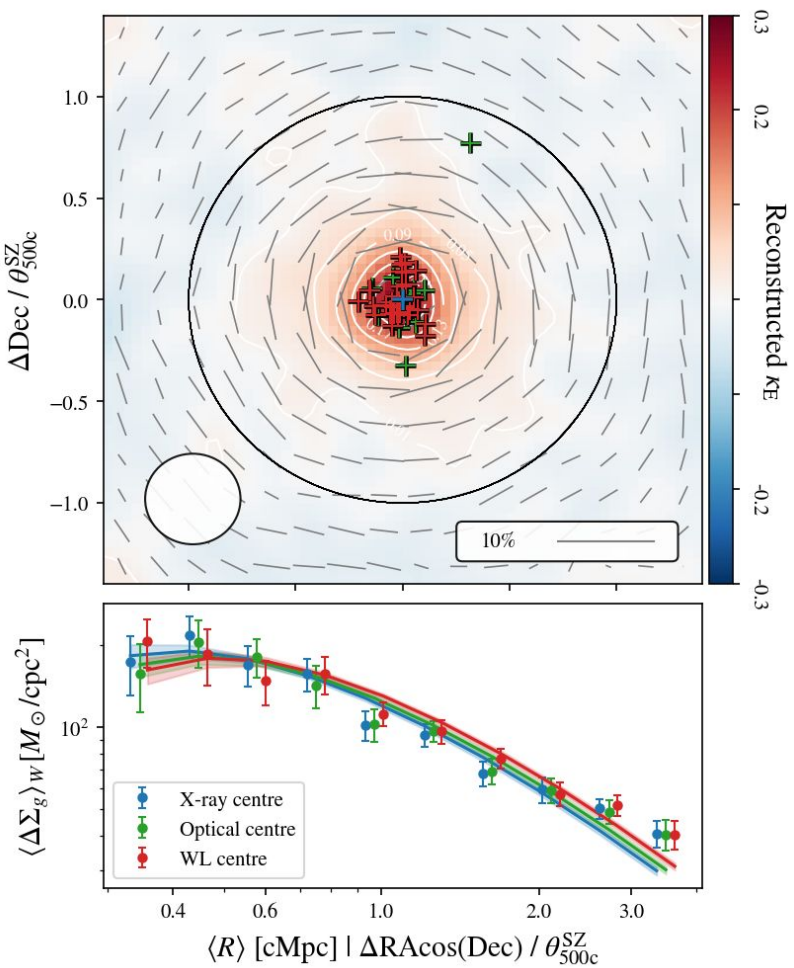

Populations

- The cluster sample is binned in population of r**adio classification** and **dynamical state**
- Categories are also defined with **radio halo sizes**
- **Miscentring** effect is shown with the WL peaks detection separation and the slope of the shear profile at low R

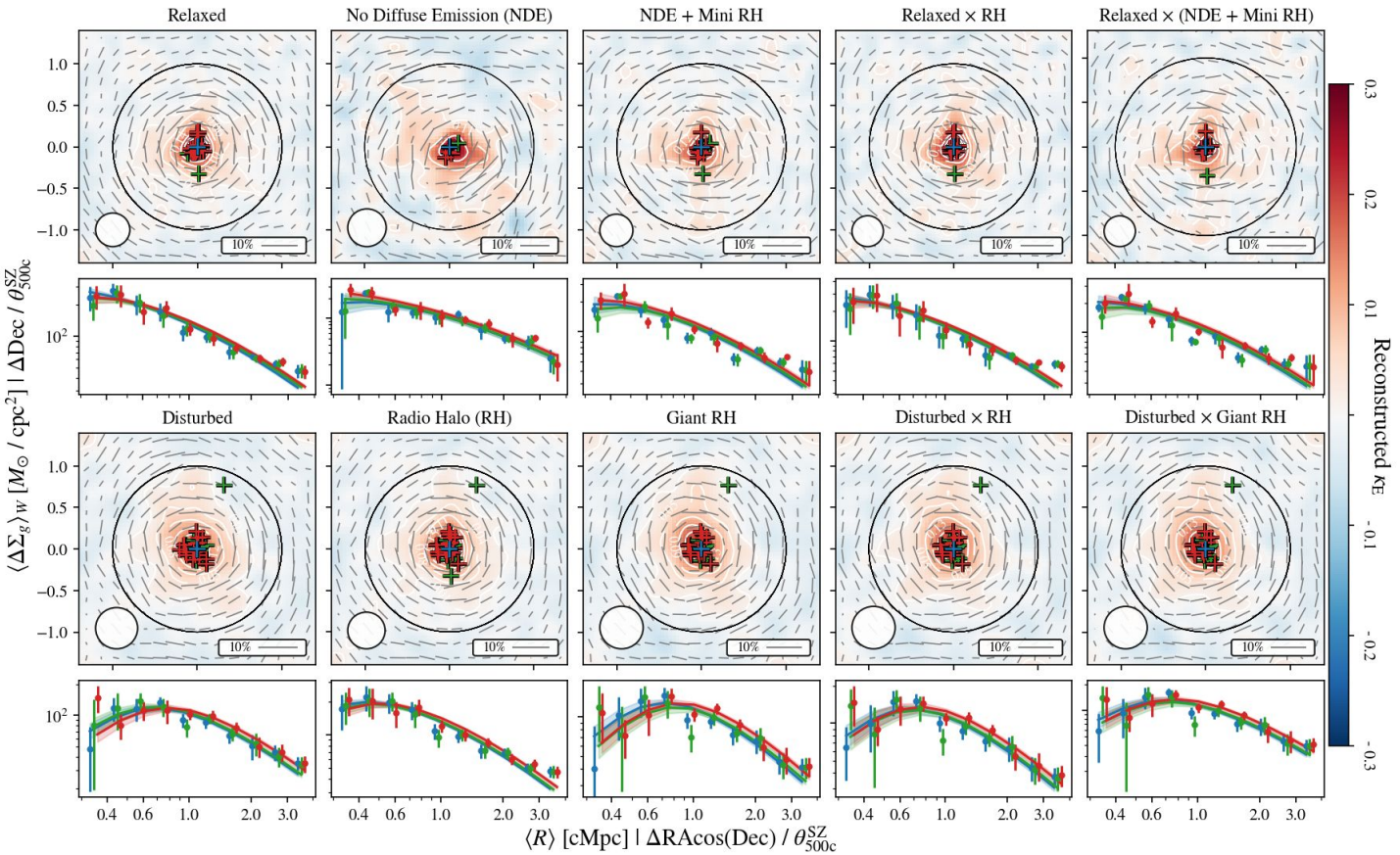

Mass vs concentration vs miscentring

X-ray centre

- To disentangle the degeneracy between **concentration** and **miscentring parameters**, each component is fitted **separately** together with the halo mass
- Concentration and miscentering are assumed to be **uncorrelated** in the model
- Results:
  - **Disturbed clusters, giant radio halos, and the combined population** show:
    - low concentration
    - high miscentring
  - **Relaxed clusters, non-detections (NDE), and mini-halo systems, and combined population** show:
    - high concentration
    - low miscentring
  - The full radio-halo population appears **mixed**, and broadly consistent with the overall sample.

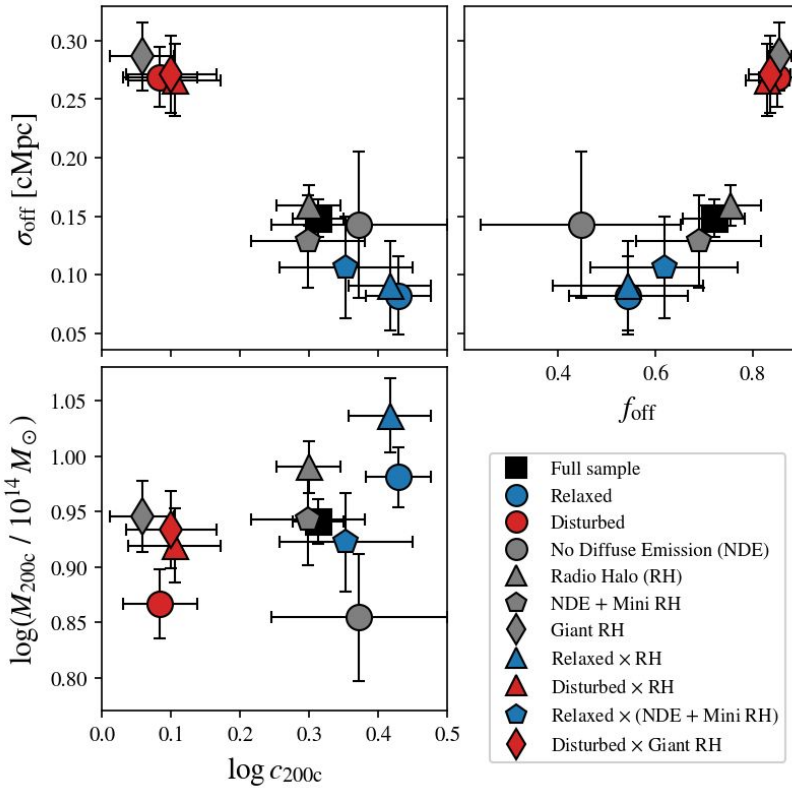

Conclusions and perspectives

Conclusions on the current work:

- We performed a **joint weak-lensing and radio analysis** of CHEX-MATE clusters, combining multi-wavelength data and mass reconstruction.
- Weak lensing provides a **robust tracer of the total cluster mass distribution**, enabling direct comparison with radio diffuse emission and X-ray morphological classifications.
- We find that:
  - **Peaks detections and centres offsets** show **systematic differences** between cluster populations
  - **Disturbed clusters and giant radio halos** show **low concentration and high miscentering**
  - **Relaxed systems and mini-halos + non diffuse emission** show **high concentration and low miscentering**
- Conclusion: the radio halo population is **mixed**, indicating **no one-to-one correlation** between the presence of radio emission and their dynamical state, but **clear connection** is established with the **radio halo size and the spatial properties** of the total mass distribution

Possible future work:

- Extend the analysis to **individual high-SNR clusters** for detailed case studies
- Measure **halo ellipticity** directly from weak-lensing mass maps
- Identify and model **substructures** within clusters
- Perform **multi-component mass fitting** and define the **merger ratio**
- Ultimately measure if substructures are **co-spatial** with:
  - radio halo and relics
  - the hot gas distribution

DR1
End 2026!